Mathematical and Computational Applications

MDPI

Article

A Mathematical Lens on the Zoonotic Transmission of Lassa Virus Infections Leading to Disabilities in Severe Cases

Yasir Ramzan [1], Hanadi Alzubadi [2], Aziz Ullah Awan [1,*], Kamel Guedri [3], Mohammed Alharthi [4] and Bandar M. Fadhl [3,5]

[1] Department of Mathematics, University of the Punjab, Lahore 54590, Pakistan; yasirramzan481@gmail.com
[2] Department of Mathematics, Umm Al-Qura University, Makkah 24382, Saudi Arabia; hhzubadi@uqu.edu.sa
[3] Mechanical Engineering Department, College of Engineering and Architecture, Umm Al-Qura University, Makkah 21955, Saudi Arabia; kmguedri@uqu.edu.sa (K.G.); bmfadhl@uqu.edu.sa (B.M.F.)
[4] Department of Mathematics, College of Sciences, University of Bisha, P.O. Box 344, Bisha 61922, Saudi Arabia; malharthy@ub.edu.sa
[5] King Salman Center for Disability Research, Riyadh 11614, Saudi Arabia
* Correspondence: aziz.math@pu.edu.pk

Abstract: This study aims to analyze the dynamics of Lassa fever transmission and its impact on the brain and spinal cord then devise and analyze preventive actions. The stability of the infection-free equilibrium point is evaluated; the model's precision is examined using empirical data; and all parameters are estimated and fitted. Subsequently, the basic reproductive number is determined, and subpopulation trends are observed over time. Sensitivity analysis is conducted to identify critical drivers influencing transmission dynamics. Two-dimensional plots visualize the impact of crucial parameters on the reproductive number. Through a comprehensive literature review and case analysis, an association between Lassa fever and various disabilities is established, including conditions such as encephalitis, hearing loss, ataxia, neuropsychiatric manifestations, meningitis, seizures, and coma. Solutions are devised and analyzed to enhance early detection, treatment, and mitigation of disease.

Keywords: mathematical application; Lassa virus; disabilities; empirical data; sensitivity analysis; optimal control

Citation: Ramzan, Y.; Alzubadi, H.; Awan, A.U.; Guedri, K.; Alharthi, M.; Fadhl, B.M. A Mathematical Lens on the Zoonotic Transmission of Lassa Virus Infections Leading to Disabilities in Severe Cases. *Math. Comput. Appl.* **2024**, *29*, 102. https://doi.org/10.3390/mca29060102

Academic Editor: Cristiana João Soares da Silva

Received: 22 October 2024
Accepted: 4 November 2024
Published: 7 November 2024

1. Introduction

The World Health Organization defines disease as a state that negatively impacts the proper operation of any human, animal, or plant organism. Illnesses in humans are commonly identified through discomfort, suffering, malfunction, or death. Infectious diseases can be transmitted directly or indirectly through microorganisms and pose significant global health concerns due to their potential to cause widespread illness and fatalities [1].

One such disease is Lassa fever, also known as Lassa hemorrhagic fever, which is a zoonotic disease that has emerged or reemerged in various West African countries, including Liberia, Ghana, Guinea, Nigeria, Côte d'Ivoire, Togo, Benin, and Sierra Leone [2,3]. Between the 3 and 30 of January 2022, Nigeria documented a total of 211 laboratory-confirmed instances of Lassa fever, leading to 40 fatalities. These cases emerged across 14 of the 36 Nigerian states and the Federal Capital Territory, covering a large portion of the country. Notably, most Lassa virus infections in humans, around 80%, are asymptomatic or have mild symptoms. The remaining 20% of cases are accompanied by febrile ailments of varying severity that can cause multiple organ malfunctions with or without bleeding. Although the overall case fatality ratio for the virus is approximately 1%, it is considerably higher for patients with severe illnesses who require hospitalization, reaching about 15%. It is primarily transmitted to humans through contact with contaminated food and household items tainted with urine or feces from Mastomys rats. Secondary human-to-human

transmission can also occur via direct contact with infected individuals' blood, secretions, organs, or other bodily fluids [4], as depicted in Figure 1.

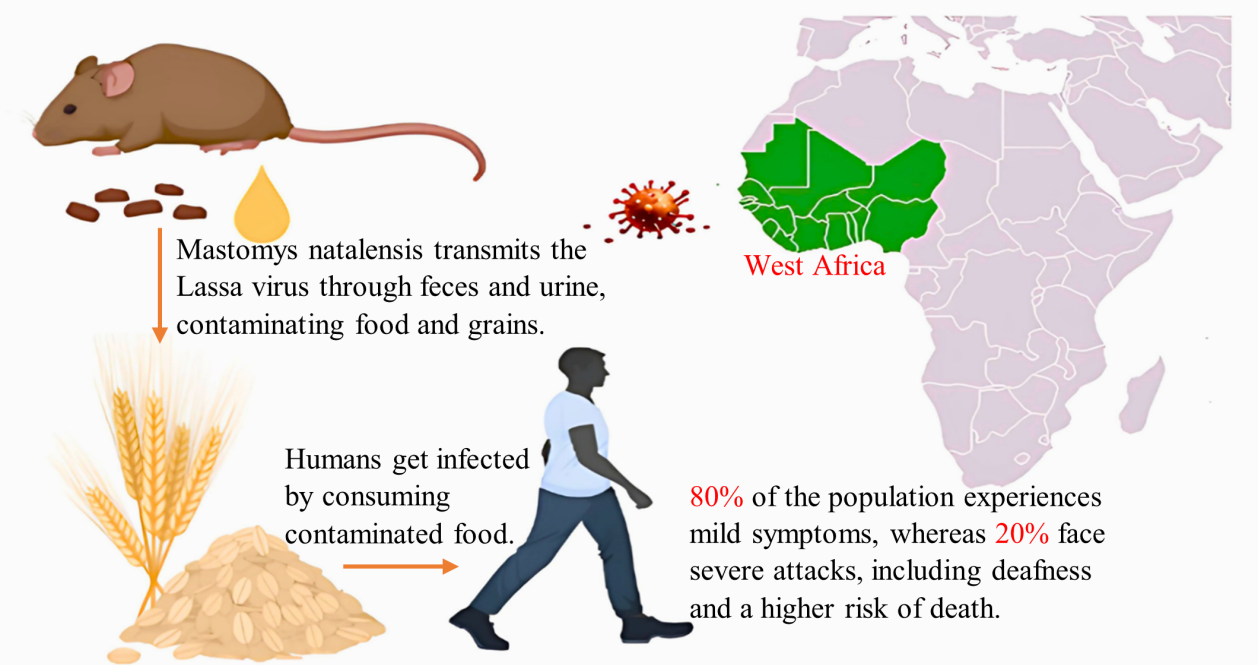

Figure 1. Transmission of Lassa virus.

The virus first targets immune cells in the nasopharynx and then spreads to nearby lymph nodes before disseminating to multiple organs. Following an incubation period of 1 to 3 weeks, the disease's progression varies widely. While most patients exhibit mild symptoms like malaise, headache, and low-grade fever, more severe cases can present a range of symptoms, including diarrhea, low blood pressure, and pulmonary edema. A small percentage, less than 20%, may exhibit oozing blood from the oropharynx, rectum, or genitals, as documented by Khan et al. [5].

Sensorineural deafness is the most common neurological disability observed in patients with Lassa fever. Reports suggest that this complication affects around 25% to one-third of individuals who survive the illness, although some studies argue that this estimation might be too high [5,6]. Interestingly, hearing loss typically occurs during the convalescent phase of the illness, even after the patient's overall recovery, indicating that an immune-related mechanism rather than a direct viral cause might be responsible for this disorder [7]. This hearing loss can affect one ear (unilateral) or both ears (bilateral) and resolves spontaneously in fewer than half of cases.

The infrequent central nervous system (CNS) disabilities caused by Lassa fever include sensorineural deafness, encephalitis (characterized by inflammation of the brain), delayed or recuperative ataxia (manifesting as a loss of coordination), subacute or prolonged neuropsychiatric manifestations (such as mania, depression, asthenia, sleep disturbances, cognitive impairments, and psychosis), meningitis (involving inflammation of the meninges surrounding the brain and spinal cord), seizures, and coma. These neurological symptoms are less common than the more typical systemic manifestations of Lassa fever [8–10].

To cope with specific issues and advance our knowledge of epidemiological circumstances, several models for different diseases have been constructed, as shown in [11–19]. Ndenda et al. [20] and Barua et al. [21] developed a mathematical model to analyze the transmission dynamics of the Lassa virus qualitatively, taking into account mildly and severely infected individuals separately. Still, their models needed to incorporate optimal control analysis. This study extends the framework of ordinary differential equations to analyze the virus' transmission among rodent and human populations, considering variability

in disease severity among individuals. Furthermore, this investigation provides a visual analysis of control strategies to prevent disabilities caused by Lassa fever, contributing to its novelty.

2. Methods

This study utilizes a diverse methodological framework, combining epidemiological modeling and biomedical investigations, to explore Lassa fever's spread patterns and neurological consequences. The primary emphasis is on devising robust preventive measures and innovative diagnostic tools.

2.1. Epidemiological Model

Mathematical modeling is one of the most essential tools for understanding disease transmission dynamics. The deterministic model's formulation involves the subdivision of the human population, $\mathbb{H}(t)$, into susceptible, $S(t)$, mildly infected, $I_m(t)$, severely infected, $I_s(t)$, and recovered individuals, $R(t)$, mathematically interpreted as

$$\mathbb{H}(t) = S(t) + I_m(t) + I_s(t) + R(t),$$

while the rodent population, $\mathbb{M}(t)$, which is categorized into susceptible rodents, $S_r(t)$, and infected rodents, $I_r(t)$, can be elucidated as

$$\mathbb{M}(t) = S_r(t) + I_r(t).$$

The rate at which the human population becomes susceptible is denoted by Π. In contrast, the relative transmissibilities from human to human in the mildly and severely infected categories are represented by β_m and β_s, respectively. The transition rate from the mild to the severe category is γ. Furthermore, the relative transmission rates from rodents to humans are denoted as α_m and α_s, while the relative recovery rates are symbolized by ρ_m and ρ_s.

For the population of rodents, Λ is taken as the recruitment rate, and ϕ represents the rate of transmission among rodents, where ν and ξ signify the mortality rates for the human and rodent populations, respectively.

The system of differential equations can be formulated based on the above description to represent the biological problem illustrated by a schematic diagram Figure 2.

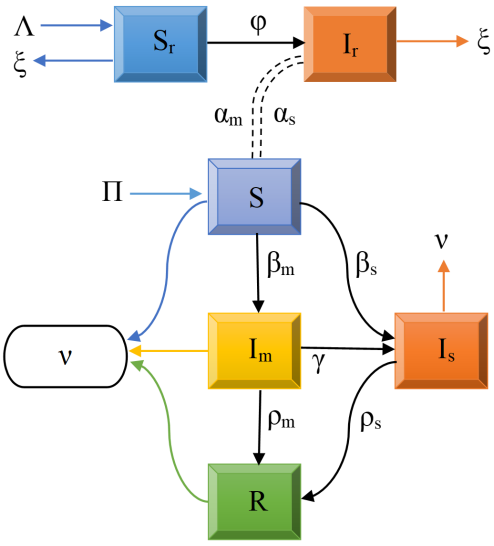

Figure 2. Schematic diagram of Model (1).

$$\begin{aligned}
\frac{dS}{dt} &= \Pi - \beta_m I_m S - \beta_s I_s S - (\alpha_m + \alpha_s) S I_r - \nu S, \\
\frac{dI_m}{dt} &= \beta_m I_m S + \alpha_m S I_r - \gamma I_m - (\nu + \rho_m) I_m, \\
\frac{dI_s}{dt} &= \beta_s I_s S + \alpha_s S I_r + \gamma I_m - (\nu + \rho_s) I_s, \\
\frac{dR}{dt} &= \rho_m I_m + \rho_s I_s - \nu R, \\
\frac{dS_r}{dt} &= \Lambda - \phi S_r I_r - \xi S_r, \\
\frac{dI_r}{dt} &= \phi S_r I_r - \xi I_r.
\end{aligned} \tag{1}$$

All the variables utilized here must remain non-negative for $t \geq 0$, as they represent the human and rodent populations. The populations of both hosts and vectors can be expressed as a set of equations:

$$\begin{aligned}
\frac{d\mathbb{H}}{dt} &= \Pi - \nu(S + I_m + I_s + R), \\
\frac{d\mathbb{M}}{dt} &= \Lambda - \xi(S_r + I_r).
\end{aligned} \tag{2}$$

The positively invariant region for Model (1) is defined as

$$\mathcal{W} = \left\{ (S, I_m, I_s, R, S_r, I_r) \in \mathbb{R}^6_+ : \quad S + I_m + I_s + R \leq \frac{\Pi}{\nu}, \quad S_r + I_r \leq \frac{\Lambda}{\xi} \right\}. \tag{3}$$

2.2. Infection-Free Equilibrium (IFE) and Basic Reproductive Number (R_0)

The infection-free equilibrium point of Model (1) can be calculated by setting the state variables representing infectious compartments equal to zero in the differential equations:

$$\mathbb{E}_0 = \left(\frac{\Pi}{\nu}, 0, 0, 0, \frac{\Lambda}{\xi}, 0 \right). \tag{4}$$

The basic reproductive number, which provides clear insight into the transmission of any infectious disease, is derived using the next-generation matrix approach. This methodology can be thoroughly grasped by delving into the theory presented in [22]. The expression for the basic reproductive number [23,24] is as follows:

$$R_0 = max[R_m, R_s, R_r], \tag{5}$$

where

$$\begin{aligned}
R_m &= \frac{(\Pi \beta_m - \gamma \nu)}{\nu^2 + \rho_m \nu}, \\
R_s &= \Pi \frac{\beta_s}{\nu^2 + \rho_s \nu}, \\
R_r &= \Lambda \frac{\phi}{\xi^2}.
\end{aligned}$$

Here, R_m and R_s denote the basic reproduction numbers for mildly and severely infected human populations, respectively, while R_r denotes the basic reproduction number for rodents. Effective public health interventions and the evaluation of disease dynamics depend on these metrics.

2.3. Stability Analysis

The use of stability analysis in mathematical models of infectious diseases offers significant insights into disease transmission and persistence dynamics. By evaluating the stability of various equilibrium points, one can better understand the possible outcomes of different control strategies. This is important as better understanding the potential consequences of various control analyses is vital for predicting the trajectory of infectious diseases and informing policies to mitigate their impact on populations.

Theorem 1. *The infection-free equilibrium point, $\mathbb{E}_0$, exhibits local asymptotic stability within the positively continuous set $\mathcal{W}$ if R_0 does not exceed unity* [25].

Proof. The local stability of infection-free equilibrium exhibits the short-living phenomenon of Lassa virus [26]. To investigate this further, the Jacobian matrix of System (1) at the IFE is computed as follows:

$$\mathcal{J}^0 = \begin{pmatrix} -\nu & -\beta_m\frac{\Pi}{\nu} & -\beta_s\frac{\Pi}{\nu} & 0 & 0 & -(\alpha_m+\alpha_s)\frac{\Pi}{\nu} \\ 0 & \beta_m\frac{\Pi}{\nu}-\gamma-(\nu+\rho_m) & 0 & 0 & 0 & \alpha_m\frac{\Pi}{\nu} \\ 0 & \gamma & \beta_s\frac{\Pi}{\nu}-(\nu+\rho_s) & 0 & 0 & \alpha_s\frac{\Pi}{\nu} \\ 0 & \rho_m & \rho_s & -\nu & 0 & 0 \\ 0 & 0 & 0 & 0 & -\xi & -\phi\frac{\Lambda}{\xi} \\ 0 & 0 & 0 & 0 & 0 & \phi\frac{\Lambda}{\xi}-\xi \end{pmatrix}. \quad (6)$$

The eigenvalues of the matrix $\mathcal{J}^0$ are

$$\begin{aligned} \lambda_1 &= -\xi, \\ \lambda_2 &= -\nu, \\ \lambda_3 &= -\frac{1}{\xi}\left(\xi^2-\Lambda\phi\right) = \xi(R_r-1), \\ \lambda_4 &= -\frac{1}{\nu}\left(\nu^2+\gamma\nu-\Pi\beta_m+\nu\rho_m\right), \\ \lambda_5 &= -\frac{1}{\nu}\left(\nu^2+\rho_s\nu-\Pi\beta_s\right). \end{aligned}$$

Both λ_1 and λ_2 exhibit a negative value, and in addition, λ_3 has a negative value if $R_r < 1$. Similarly, λ_4 and λ_5 have negative values if $R_m < 1$ and $R_s < 1$, respectively. When the eigenvalues are negative, a stable infection-free equilibrium will eventually arise, and the infection dynamics will gradually decrease. □

The consequences of Theorem 1 hold substantial significance in the battle against Lassa fever. When the condition $R_0 < 1$ is met, alongside an initial infected population falling within the bounds specified by IFE (4), there emerges a feasible opportunity to eradicate the infection from the entire population. However, if $R_0 > 1$, the disease will likely persevere.

The task of achieving infection eradication proves to be immensely challenging, irrespective of the initial infected population's size. Consequently, comprehensively assessing global stability at the IFE becomes a formidable undertaking. The global stability findings outlined in [27] are brought into play to address this.

Theorem 2. *The infection-free equilibrium point, $\mathbb{E}_0$, exhibits global asymptotic stability within the positively continuous set $\mathcal{W}$ if R_0 does not exceed unity* [25].

It suffices to verify the Castillo–Chavez conditions, presented in [27], to investigate the global asymptotic stability at IFE. The state variables in System (1) are $\mathbb{X}_1 = (S, S_r)$ and $\mathbb{X}_2 = (I_m, I_s, I_r)$ and the infection-free equilibrium is $\mathbb{X}_1^* = \left(\frac{\Pi}{\nu}, \frac{\Lambda}{\xi}\right)$. The system of linear equations can be solved through the following means:

$$\begin{aligned} \frac{dS}{dt} &= \Pi - \nu S, \\ \frac{dS_r}{dt} &= \Lambda - \xi S_r, \end{aligned}$$

where we have

$$\begin{aligned} S &= \frac{\Pi}{\nu} - \left(\frac{\Pi}{\nu} - S(0)\right)e^{-\nu t}, \\ S_r &= \frac{\Lambda}{\xi} - \left(\frac{\Lambda}{\xi} - S_r(0)\right)e^{-\xi t}. \end{aligned}$$

The aforementioned equations tend towards the limits $\frac{\Pi}{\nu}$ and $\frac{\Lambda}{\xi}$, respectively, as t approaches infinity, regardless of the initial values of $S(0)$ and $S_r(0)$. Consequently, $\mathbb{X}_1^* = \left(\frac{\Pi}{\nu}, \frac{\Lambda}{\xi}\right)$ is considered globally asymptotically stable. Moreover, it can be asserted that

$$\mathbb{G}(\mathbb{X}_1, \mathbb{X}_2) = \begin{pmatrix} \beta_m I_m S + \alpha_m S I_r - \gamma I_m - (\nu + \rho_m) I_m \\ \beta_s I_s S + \alpha_s S I_r + \gamma I_m - (\nu + \rho_s) I_s \\ \phi S_r I_r - \xi I_r \end{pmatrix}.$$

define $\mathbb{A}$ and $\mathbb{A}\mathbb{X}_2$ as follows:

$$\mathbb{A} = \begin{pmatrix} \beta_m \frac{\Pi}{\nu} - \gamma - (\nu + \rho_m) & 0 & \frac{\alpha_m \Pi}{\nu} \\ \gamma & \beta_s \frac{\Pi}{\nu} - (\nu + \rho_s) & \frac{\alpha_s \Pi}{\nu} \\ 0 & 0 & \frac{\phi \Lambda}{\xi} - \xi \end{pmatrix},$$

$$\mathbb{A}\mathbb{X}_2 = \begin{pmatrix} \frac{1}{\nu}\Pi\alpha_m I_r - I_m\left(\gamma + \nu + \rho_m - \frac{1}{\nu}\Pi\beta_m\right) \\ \gamma I_m - I_s\left(\nu + \rho_s - \frac{1}{\nu}\Pi\beta_s\right) + \frac{1}{\nu}\Pi\alpha_s I_r \\ \left(\Lambda\frac{\phi}{\xi} - \xi\right) I_r \end{pmatrix}.$$

The matrix $\mathbb{A}$ possesses off-diagonal non-negative entries, classifying it as an M-matrix. As a result, $\hat{\mathbb{G}}$ can be derived from the expression $\mathbb{A}\mathbb{X}_2 - \mathbb{G}$.

$$\hat{\mathbb{G}}(\mathbb{X}_1, \mathbb{X}_2) = \begin{pmatrix} \left(\frac{\Pi}{\nu} - S\right)\beta_m I_m + \left(\frac{\Pi}{\nu} - S\right)\alpha_m I_r \\ \left(\frac{\Pi}{\nu} - S\right)\beta_s I_s + \left(\frac{\Pi}{\nu} - S\right)\alpha_s I_r \\ \left(\frac{\Lambda}{\xi} - S_r\right)\phi I_r \end{pmatrix}.$$

It is clear that $\hat{\mathbb{G}}(\mathbb{X}_1, \mathbb{X}_2)$ is non-negative, where $0 \leq S \leq \mathbb{H}$ and $0 \leq S_r \leq \mathbb{M}$.

2.4. Parameter Estimation and Model Fitting

The precise estimation of parameter values remains critical in epidemiological research, ensuring the accuracy of predictions. Validating Model (1) against empirical data is pivotal for obtaining reliable results, achieved through fitting it to empirical data, offering crucial insights into predictive accuracy. This study utilized Lassa fever cases reported in Nigeria and confirmed [4], from weeks one to four in 2022, to estimate parameters, separately assessing mild and severe cases. Notably, the escalating counts of confirmed cases underscore the urgent need for effective disease control measures in the community. The estimated parameter values, evaluated for mild and severe cases and presented in Tables 1 and 2, respectively, are calibrated against authentic data, acknowledging Nigeria's average life expectancy of 55.44 years [28]. Figure 3 represents the tally of confirmed cases in Nigeria—comparing actual versus estimated numbers.

Table 1. Estimated parameter values for the mildly infected population.

Notations	Values	Discription	Source
Π	75,806.6	Birth rate of humans per week	[28,29]
ν	3.46875×10^{-4}	Rate at which humans die naturally	[28]
β_m	4.0×10^{-9}	Rate of mild infections through humans	fitted
β_s	1.5×10^{-9}	Rate of severe infections through humans	fitted
α_m	$[1.0 \times 10^{-8}, 4.69 \times 10^{-8}]$	Rate of mild infections through rodents	fitted
α_s	0.0865	Rate of severe infections through rodents	fitted
γ	0.3	Rate of being severely infected from mild infection	fitted
ρ_m	0.2	Rate at which humans recover from mild infection	fitted
ρ_s	0.1	Rate at which humans recover from severe infection	fitted
Λ	125,000	Birth rate of rodents per week	assumed
ϕ	1.0×10^{-6}	Rate of infection between rodents	fitted
ξ	0.2	Rate at which rodents die naturally	fitted

Table 2. Estimated parameter values for the severely infected population.

Notations	Values	Discription	Source
Π	75,806.6	Birth rate of humans per week	[28,29]
ν	3.46875×10^{-4}	Rate at which humans die naturally	[28]
β_m	1.0×10^{-11}	Rate of mild infections through humans	fitted
β_s	1.0×10^{-11}	Rate of severe infections through humans	fitted
α_m	$[1.0 \times 10^{-13}, 7.4 \times 10^{-9}]$	Rate of mild infections through rodents	fitted
α_s	1.0×10^{-15}	Rate of severe infections through rodents	fitted
γ	1.0×10^{-4}	Rate of being severely infected from mild infection	fitted
ρ_m	5.0×10^{-4}	Rate at which humans recover from mild infection	fitted
ρ_s	$[2.49 \times 10^{-3}, 7.7 \times 10^{-2}]$	Rate at which humans recover from severe infection	fitted
Λ	125,000	Birth rate of rodents per week	assumed
ϕ	1.0×10^{-6}	Rate of infection between rodents	fitted
ξ	0.2	Rate at which rodents die naturally	fitted

Utilizing the count of confirmed incidences of Lassa Fever reported in Nigeria during weeks one (starting from 2 January) through four (starting from 23 January) in the year 2022 [4], the reproductive number for transmissions between humans and rodents is evaluated based on mild and severe cases in the human population. The computed reproductive number for the population infected with mild symptoms ranges from 2.46248 to 2.86586. Likewise, the range for the population with severe symptoms is 0.0282547 to 3.26679, whereas the reproductive number for rodents is 3.125.

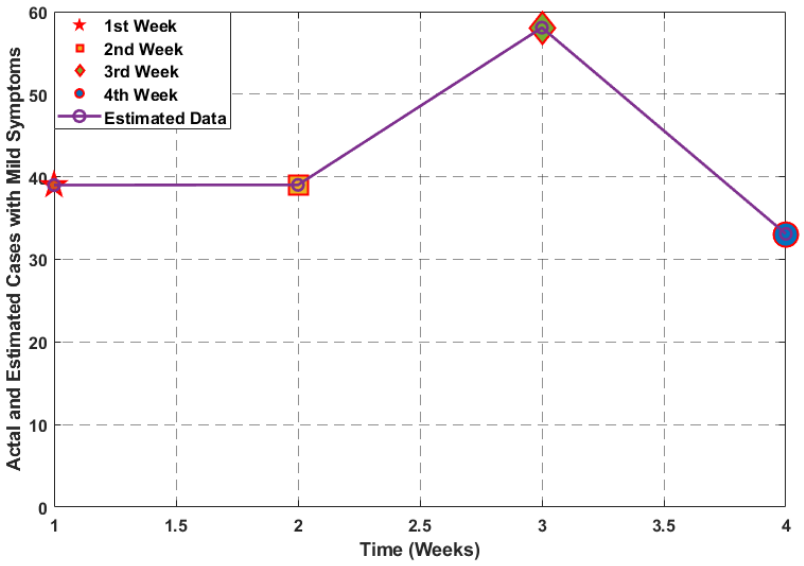

(**a**)

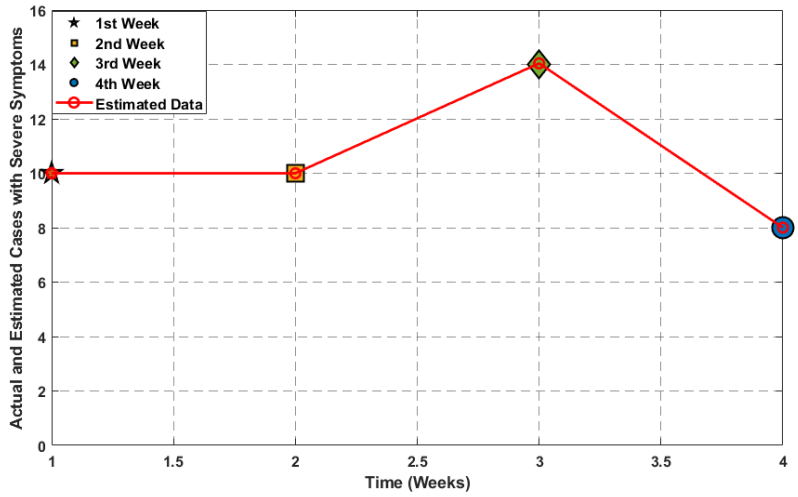

(**b**)

Figure 3. Visualization depicting the tally of confirmed cases in Nigeria—comparing actual versus estimated numbers. The various marker shapes denote actual cases per week, while the line represents estimated data. Data are categorized as (**a**) mild and (**b**) severe cases, spanning four weeks from 2 January to 30 January 2022 [4]. The estimated data exhibit a close resemblance to the actual data.

2.5. Population Dynamics

This section explains the estimated parameters and clarifies the intricate interactions between various factors that help spread the virus throughout the population. The Figures 4 and 5 makes the information presented transparent, which also helps illustrate how the virus spreads over time. This methodology is necessary to give a more complete view of the epidemiological scenario being studied.

Actual epidemiological data spanning four weeks in Nigeria are employed as the foundation for parameter estimation within the model, followed by implementing the RK4 method to solve the model. This approach yields outcomes for estimated and fitted parameters, which form the basis for a comprehensive discussion on the model's solution and its implications for understanding the evolving dynamics of the disease over time.

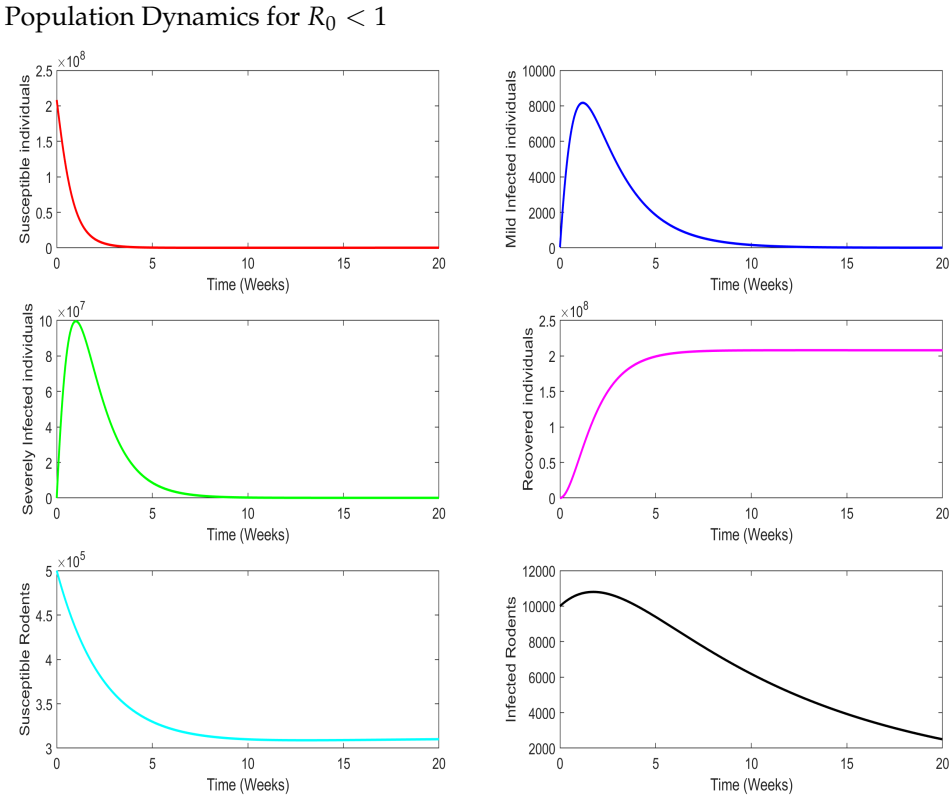

Figure 4. Illustration depicting the population dynamics using estimated values of the parameters for $R_0 < 1$, where $R_m = 0.8940$, $R_s = 0.9110$, and $R_r = 0.7812$.

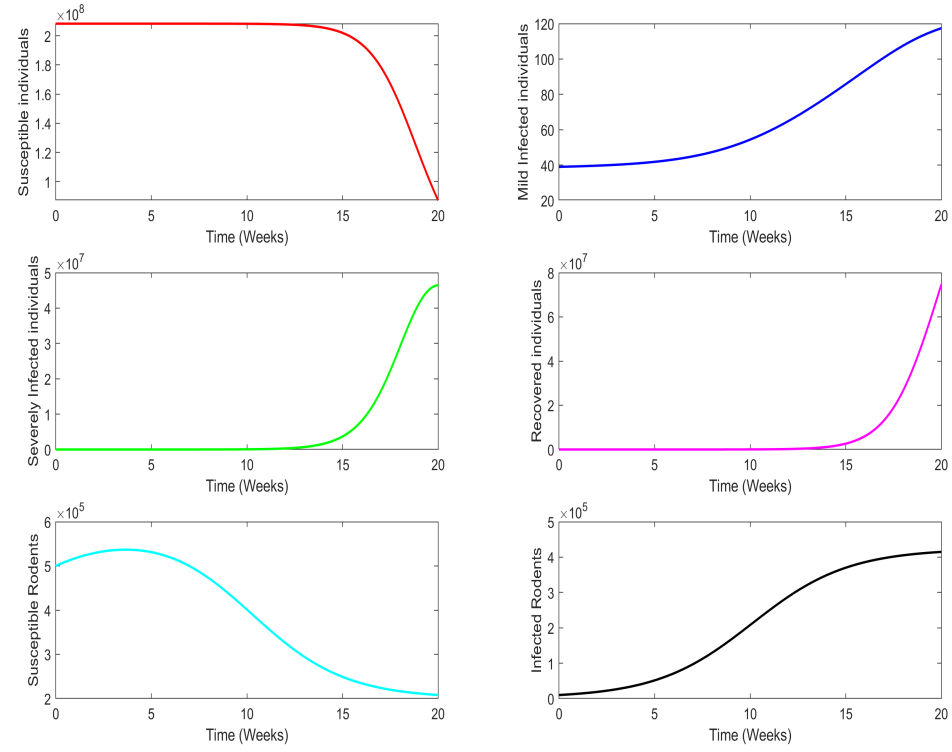

Figure 5. Illustration depicting the population dynamics using estimated values of the parameters for $R_0 > 1$, where $R_m = 2.3148$, $R_s = 2.42288$, and $R_r = 3.1250$.

2.6. Sensitivity Analysis

Sensitivity analysis is essential for assessing how parameter fluctuations like population density, transmission rates, or intervention strategies affect the model's results. This technique helps determine which parameters affect forecasts the most. Providing insights into uncertainty enables researchers and policymakers to prioritize interventions and devise strategies for controlling disease.

Sensitivity Indices

Sensitivity indices offer a way of measuring the shift in the state variable brought about by parameter variations. Chitnis et al. have devised a method involving partial derivatives to compute sensitivity indices, as detailed in their work [30]. The mathematical expression for these indices is as follows:

$$\Gamma_x^{R0} = \frac{\partial R_0}{\partial x} \times \frac{x}{R_0}. \tag{7}$$

Analyzing the data presented in Tables 3 and 4, it becomes evident that there is a direct correlation between virus transmission and trends observed in the parameters β_m, β_s, and ϕ. Conversely, virus transmission is inversely related to the negative values associated with the parameters γ, ρ_m, ρ_s, and ξ. Among these sensitivity indices, ξ exhibits the most significant negative value, representing the rate at which rodents die naturally.

Table 3. Sensitivity indices using estimated parameter values for the mildly infected population.

Parameters	Discription	Sensitivity Index	Sign
β_m	Rate of mild infections through humans	1.5225	+ve
β_s	Rate of severe infections through humans	1	+ve
γ	Rate of being severely infected from mild infection	−0.52250	−ve
ρ_m	Rate at which humans recover from mild infection	−0.99822	−ve
ρ_s	Rate at which humans recover from severe infection	−0.99654	−ve
ϕ	Rate of infections between rodents	1	+ve
ξ	Rate at which rodents die naturally	−2	−ve

Table 4. Sensitivity indices using estimated parameter values for the severely infected population.

Parameters	Discription	Sensitivity Index	Sign
β_m	Rate of mild infections through humans	1.0480	+ve
β_s	Rate of severe infections through humans	1	+ve
γ	Rate of being severely infected from mild infection	−0.047952	−ve
ρ_m	Rate at which humans recover from mild infection	−0.59041	−ve
ρ_s	Rate at which humans recover from severe infection	$[-0.99552, -0.87773]$	−ve
ϕ	Rate of infections between rodents	1	+ve
ξ	Rate at which rodents die naturally	−2	−ve

Graphical representations of these observations can be found in Figures 6 and 7. Notably, each positive index resulting from the sensitivity analysis directly increases the disease threshold quantity and vice versa.

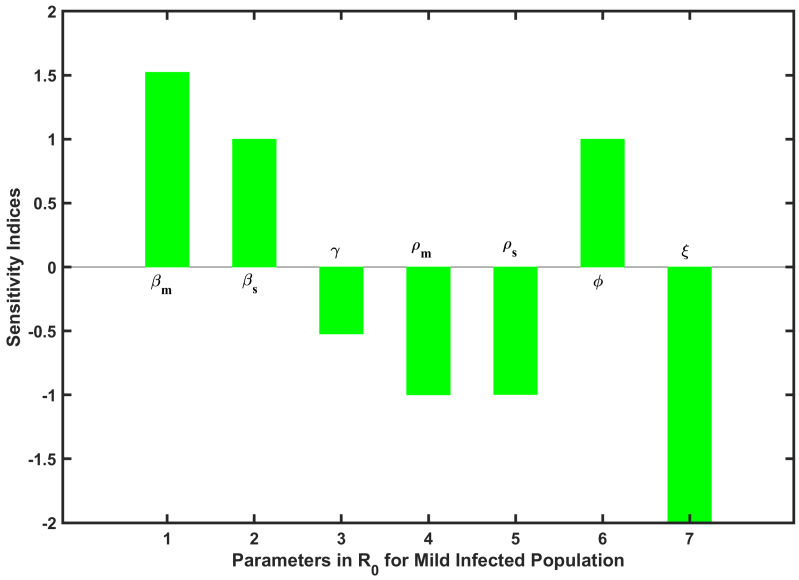

Figure 6. Visual illustration of sensitivity indices using mildly infected population.

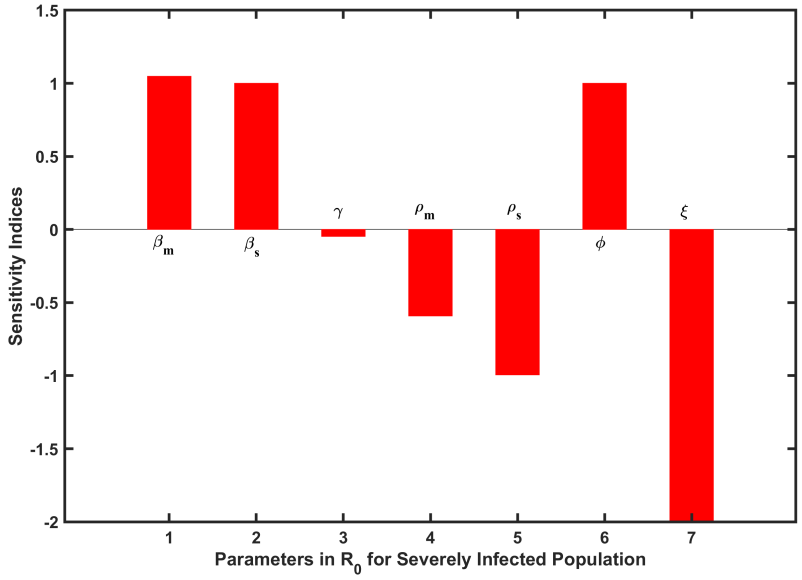

Figure 7. Visual illustration of sensitivity indices using severely infected population.

The sensitivity analysis reveals that the index of the parameter ϕ, which represents the rate of transmission among rodents, is $+1$. This means that any change in its value causes R_0 to climb or fall because of a direct relation. The natural mortality rate of rats, marked by the parameter ξ, also exhibits a sensitivity index of -2, meaning that a change in its value results in a reverse shift in R_0 because of an inverse relation.

2.7. Relationship Between Significant Parameters and the Basic Reproductive Number

The contour plot depicts the influence of threshold parameters on R_0. This approach offers an effective way to understand how changing these parameters affects disease transmission potential. The contour plots in Figure 8 vividly display reproductive dynamics by manipulating two parameters.

Figure 8a illustrates the correlation between the mild infection rate among humans and the recovery rate from mild infections. These are represented by the parameters β_m and

ρ_m, respectively, and their impact on R_0 is depicted. The results underscore the significance of diminishing the mild infection rate among humans to a level below 4×10^{-9} while concurrently ensuring an elevation in the recovery rate from mild infections to keep it above 0.573819 to continue fulfilling the condition $R_0 < 1$. Similarly, Figure 8b portrays the influence of the severe infection rate among humans, denoted as β_s, and the recovery rate from severe infections, denoted as ρ_s, on R_0. The findings indicate that curtailing the severe infection rate among humans to less than 1.5×10^{-9} and elevating the recovery rate from severe infections to above 0.327465 could contribute to keeping the reproductive number below unity. Figure 8c,d similarly present analogous results concerning the parameter values required to keep R_0 below unity.

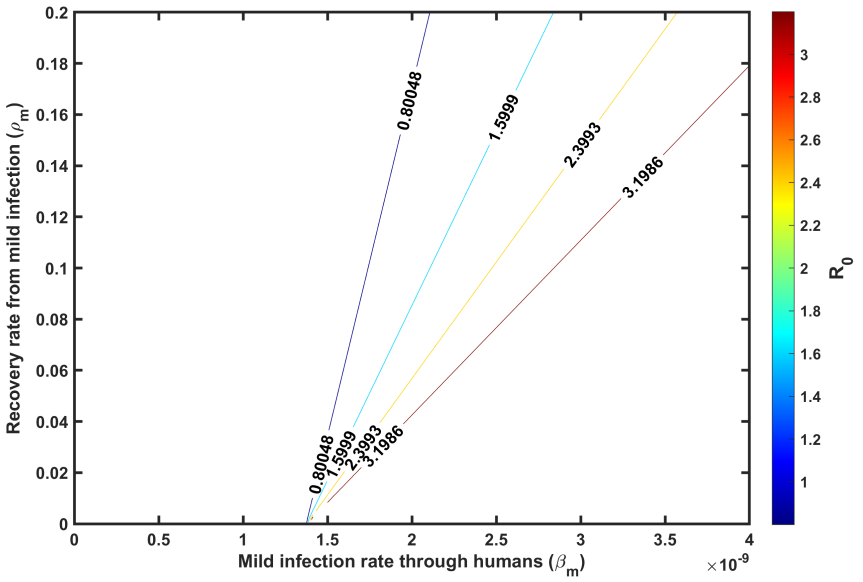

(**a**) R_0 vs. β_m and ρ_m

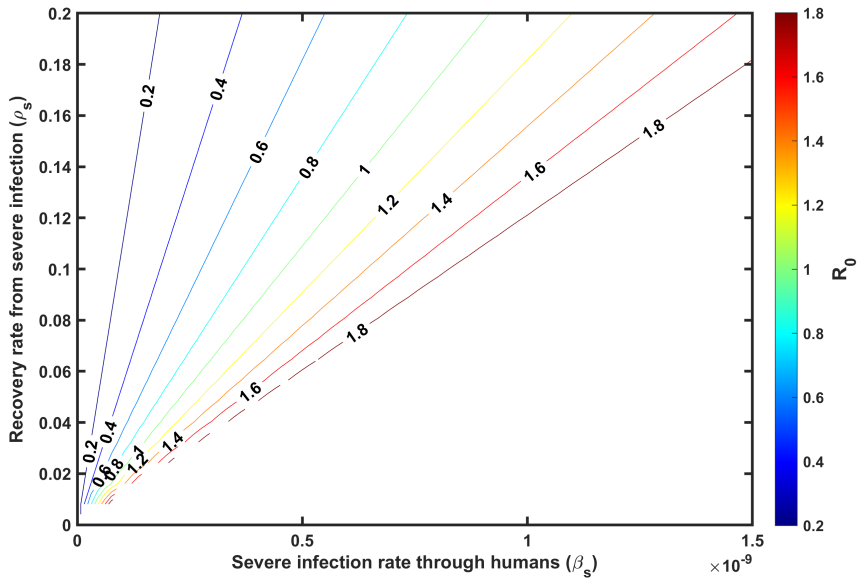

(**b**) R_0 vs. β_s and ρ_s

Figure 8. *Cont.*

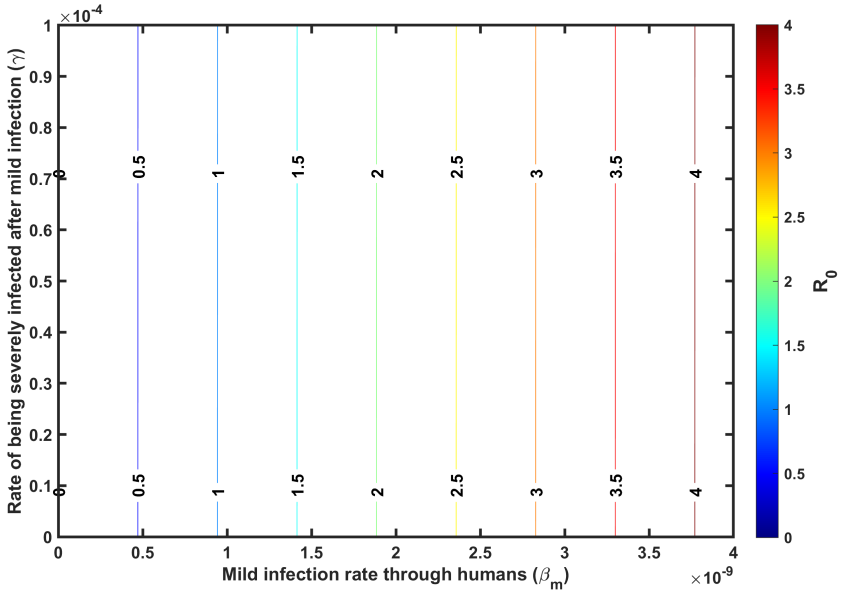

(**c**) R_0 vs. β_m and γ

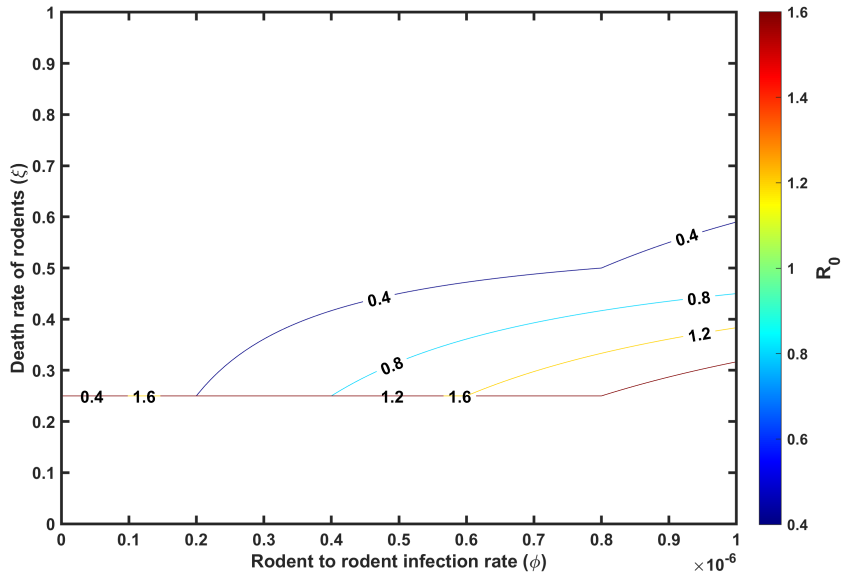

(**d**) R_0 vs. ϕ and ξ

Figure 8. Contour plot depicting the influence of parameters on R_0.

The outcomes imply that an effective control strategy should encompass reductions in both the mild and severe infection rates among humans (β_m and β_s, respectively) as well as augmentations in the recovery rates (ρ_m and ρ_s, respectively) for individuals with mild and severe infections. This is crucial for keeping R_0 below unity. An increase in the likelihood of transmission would result in a higher reproductive number. On the other hand, reducing both β_m and β_s while keeping ρ_m and ρ_s constant would cause the reproductive number to decrease.

To make R_0 less than unity, it is imperative to keep $\beta_m < 4 \times 10^{-9}$ and $\beta_s < 1.5 \times 10^{-9}$. This highlights that tweaking one transmission parameter will not greatly lower R_0. To stop the spread of viruses within the community, it is critical to have policies addressing both human–rodent transmission risks and possibilities.

2.8. Optimal Control

This section articulates three time-varying dynamic control factors, marked by the notations $\mathbb{C}_1$, $\mathbb{C}_2$, and $\mathbb{C}_3$, that are employed in Model (1) within the domain of optimizing intervention approaches for the eradication of disease. These factors use nanotechnology to enhance the virus' dissemination across the community. Below are descriptions of various dynamic control factors:

- The control approach $\mathbb{C}_1$ emphasizes maintaining cleanliness and raising community awareness. To check if these strategies effectively eliminate the Lassa virus, $\mathbb{C}_1$ is set to 1. In contrast, assigning a value of 0 to this parameter nullifies the effectiveness of these strategies. Therefore, accurately putting these preventive measures into action is crucial for eliminating the Lassa virus.
- The control approach represented by $\mathbb{C}_2$ uses nanotechnology to improve Lassa virus patient diagnosis and care. In milder instances, nanoparticles are utilized to lessen negative impacts and enhance the effectiveness of antiviral medications. Nanosensors are essential for quickly conveying illness data and supporting accurate treatment decisions during emergencies. Furthermore, nanotechnology makes protective equipment creation possible, as well as medical imaging improvements, vaccination developments, and immunological modulation. Meningitis, encephalitis, auditory impairment, neuropathy, visual issues, cognitive difficulties, organ dysfunction, paralysis, convulsions, and behavioral disorders are among the neurological side effects linked to Lassa fever.
- One novel approach based on nanotechnology to reduce the spread of viruses among vulnerable rats is represented by the control variable $\mathbb{C}_3$. Creating nano-materials to discourage rodent occupancy in certain areas is just one method in this broad plan. Additionally, precise and careful management of rodent populations can be made easier by nanoparticles containing specific poisonous agents or contraceptives. An accurate and efficient way to manage rodent populations is through novel obstacles, traps, and nanotechnologies that alter rodent behavior. The promise of nanotechnology makes the efficacious control and management of rodent-related diseases possible, as demonstrated by these pragmatic applications.

A control model for Lassa Fever management can be constructed utilizing the previous descriptions. This model involves three variables that change over time, outlined as follows:

$$\begin{aligned}
\frac{dS}{dt} &= \Pi - \beta_m I_m S - \beta_s I_s S - (1-\mathbb{C}_1)(\alpha_m + \alpha_s) S I_r - \nu S,\\
\frac{dI_m}{dt} &= \beta_m I_m S + (1-\mathbb{C}_1)\alpha_m S I_r - \gamma I_m - (\nu + \rho_m + \theta_1 \mathbb{C}_2) I_m,\\
\frac{dI_s}{dt} &= \beta_s I_s S + (1-\mathbb{C}_1)\alpha_s S I_r + \gamma I_m - (\nu + \rho_s + \theta_2 \mathbb{C}_2) I_s,\\
\frac{dR}{dt} &= (\rho_m + \theta_1 \mathbb{C}_2) I_m + (\rho_s + \theta_2 \mathbb{C}_2) I_s - \nu R,\\
\frac{dS_r}{dt} &= \Lambda(1-\mathbb{C}_3) - \phi S_r I_r - \xi S_r - \theta_3 \mathbb{C}_3 S_r,\\
\frac{dI_r}{dt} &= \phi S_r I_r - \xi I_r - \theta_3 \mathbb{C}_3 I_r.
\end{aligned} \tag{8}$$

The purpose of this model is to reduce the transmission of the Lassa virus among individuals and rodents in the community using three controls. This objective will be achieved while maintaining cost-effectiveness. To achieve this goal, the objective functional is defined as follows:

$$\mathcal{F}(\mathbb{C}_i) = \int_0^{t_f} \left(A_1 I_m + A_2 I_s + A_3 S_r + A_4 I_r + \frac{1}{2} \sum_{i=1}^{3} B_i \mathbb{C}_i^2(t) \right) dt, \tag{9}$$

where t_f denotes the ultimate execution time of the control, and $t \in [0, t_f]$ represents the constant weight factors A_i $(i = 1, 2, 3, 4)$ and B_i $(i = 1, 2, 3)$, while $\mathbb{C}_i$ represents the total cost associated with the control variables for $i = 1, \ldots, 3$. The function $\frac{B_1\mathbb{C}_1^2}{2}$ represents cost control for elevating community awareness and encouraging good hygiene practices. In contrast, $\frac{B_2\mathbb{C}_2^2}{2}$ constitutes the cost control functions for diagnosing and treating disabilities caused by Lassa fever through nanotechnology. Similarly, the term $\frac{B_3\mathbb{C}_3^2}{2}$ signifies the cost control functions related to the utilization of a nanotechnological approach for controlling virus transmission via rodents. To address the given minimization dilemma, it is essential to ascertain the optimal control, denoted as $\mathbb{C}^* = \left(\mathbb{C}_1^*, \mathbb{C}_2^*, \mathbb{C}_3^*\right)$:

$$\mathcal{F}(\mathbb{C}_1^*, \mathbb{C}_2^*, \mathbb{C}_3^*) = min\{\mathcal{F}(\mathbb{C}_1, \mathbb{C}_2, \mathbb{C}_3) : \mathbb{C}_1, \mathbb{C}_2, \mathbb{C}_3 \in \Omega\}. \tag{10}$$

Define a set Ω as

$$\Omega = \left\{(\mathbb{C}_1, \mathbb{C}_2, \mathbb{C}_3) : 0 \leq \mathbb{C}_1(t), \mathbb{C}_2(t), \mathbb{C}_3(t) \leq 1, t \in [0, t_f]\right\}.$$

Pontryagin's maximum principle reconfigures the task of reducing controls (10) within the optimal control system (8) into a pointwise challenge of minimizing the Hamiltonian. This conversion has been extensively explored in the literature [31], delineating the resultant Hamiltonian equation as $\mathcal{H}$.

$$\mathcal{H} = A_1 I_m + A_2 I_s + A_3 S_r + A_4 I_r + \frac{1}{2}\sum_{i=1}^{3} B_i \mathbb{C}_i^2(t) + \sum_{i=1}^{6} \sigma_i \mathcal{M}_i. \tag{11}$$

In this context, $\mathcal{M}_i$ for i ranging from 1 to 6 symbolizes the expressions on the right-hand side of the differential equations that dictate the behavior of the state variables in System (8). Meanwhile, σ_i, corresponding to values of i from 1 to 6, denotes the adjoint functions linked to the state variables within the control model. The expanded version of the Hamiltonian equation is articulated as follows:

$$\begin{aligned}
\mathcal{H} &= A_1 I_m + A_2 I_s + A_3 S_r + A_4 I_r + \frac{1}{2} B_1 \mathbb{C}_1^2 + \frac{1}{2} B_2 \mathbb{C}_2^2 + \frac{1}{2} B_3 \mathbb{C}_3^2 \\
&+ \sigma_1(\Pi - \beta_m I_m S - \beta_s I_s S - (1 - \mathbb{C}_1)(\alpha_m + \alpha_s) S I_r - \nu S) \\
&+ \sigma_2(\beta_m I_m S + (1 - \mathbb{C}_1)\alpha_m S I_r - \gamma I_m - (\nu + \rho_m + \theta_1 \mathbb{C}_2) I_m) \\
&+ \sigma_3(\beta_s I_s S + (1 - \mathbb{C}_1)\alpha_s S I_r + \gamma I_m - (\nu + \rho_s + \theta_2 \mathbb{C}_2) I_s) \\
&+ \sigma_4((\rho_m + \theta_1 \mathbb{C}_2) I_m + (\rho_s + \theta_2 \mathbb{C}_2) I_s - \nu R) \\
&+ \sigma_5(\Lambda(1 - \mathbb{C}_3) - \phi S_r I_r - \xi S_r - \theta_3 \mathbb{C}_3 S_r) \\
&+ \sigma_6(\phi S_r I_r - \xi I_r - \theta_3 \mathbb{C}_3 I_r).
\end{aligned}$$

The theorem presented below outlines the criteria for controls that meet the objective of minimizing the problem (10). It is important to note that the approach used in this study is based on the methods described in [32,33].

Theorem 3. *If $\mathbb{C}_1^*, \mathbb{C}_2^*$, and $\mathbb{C}_3^* \in \Omega$ are specific control variables that hold true for (10) with respect to the associated model, Model (8), then there exists a set of functions, $\sigma_1(t), \sigma_2(t), \ldots, \sigma_6(t)$, that meet the requirements of the subsequent system:*

$$\begin{aligned}
\frac{d\sigma_1}{dt} &= \nu\sigma_1 + (\sigma_1-\sigma_2)\beta_m I_m + (\sigma_1-\sigma_3)\beta_s I_s + (\sigma_1-\sigma_2)\alpha_m I_r + (\sigma_1-\sigma_3)\alpha_s I_r \\
&\quad - (\sigma_1-\sigma_2)\alpha_m I_r u_1 - (\sigma_1-\sigma_3)\alpha_s I_r u_1, \\
\frac{d\sigma_2}{dt} &= -A_1 + (\sigma_2-\sigma_3)\gamma - \sigma_4(\rho_m+\theta_1 u_2) + \sigma_2(\nu+\rho_m+\theta_1 u_2) + (\sigma_1-\sigma_2)\beta_m S, \\
\frac{d\sigma_3}{dt} &= -A_2 + (\sigma_1-\sigma_3)\beta_s S + \sigma_3(\nu+\rho_s+\theta_2 u_2) - \sigma_4(\rho_s+\theta_2 u_2), \\
\frac{d\sigma_4}{dt} &= \nu\sigma_4, \\
\frac{d\sigma_5}{dt} &= \xi\sigma_5 - A_3 + \phi\sigma_5 I_r - \phi\sigma_6 I_r + \theta_3\sigma_5 u_3, \\
\frac{d\sigma_6}{dt} &= -A_4 + \xi\sigma_6 + (\sigma_1-\sigma_2)\alpha_m S + (\sigma_1-\sigma_3)\alpha_s S + (\sigma_5-\sigma_6)\phi S_r + \theta_3\sigma_6 u_3 \\
&\quad - (\sigma_1-\sigma_2)u_1\alpha_m S - (\sigma_1-\sigma_3)u_1\alpha_s S,
\end{aligned}$$

subject to the transversality conditions $\sigma_i(t_f) = 0$ *for all* $i = 1, 2, \ldots, 6$. *Hence, the optimal control* $\Omega = (\mathbb{C}_1^*, \mathbb{C}_2^*, \mathbb{C}_3^*)$ *is given by*

$$\mathbb{C}_1^* = \min\left\{\max\left\{0, \frac{(\alpha_m(\sigma_2-\sigma_1)+\alpha_s(\sigma_3-\sigma_1))SI_r}{B_1}\right\}, 1\right\}, \tag{12}$$

$$\mathbb{C}_2^* = \min\left\{\max\left\{0, \frac{(\sigma_2-\sigma_4)\theta_1 I_m + (\sigma_3-\sigma_4)\theta_1 I_s}{B_2}\right\}, 1\right\}, \tag{13}$$

$$\mathbb{C}_3^* = \min\left\{\max\left\{0, \frac{\Lambda\sigma_5 + \theta_3\sigma_6 I_r + \theta_3\sigma_5 S_r}{B_3}\right\}, 1\right\}. \tag{14}$$

Proof. Expanding on the approach detailed in [32], Pontryagin's maximum principle can be utilized to establish the conditions for the existence of an optimal control problem, which entails an assessment of the Hamiltonian function's partial derivatives with respect to the state variables. Consequently, this process enables the derivation of the necessary conditions that the adjoint variables must fulfill, outlined as follows:

$$\begin{aligned}
&\frac{d\sigma_1}{dt} = -\frac{\partial\mathcal{H}}{\partial S}, \quad \frac{d\sigma_2}{dt} = -\frac{\partial\mathcal{H}}{\partial I_m}, \quad \frac{d\sigma_3}{dt} = -\frac{\partial\mathcal{H}}{\partial I_s}, \\
&\frac{d\sigma_4}{dt} = -\frac{\partial\mathcal{H}}{\partial R}, \quad \frac{d\sigma_5}{dt} = -\frac{\partial\mathcal{H}}{\partial S_r}, \quad \frac{d\sigma_6}{dt} = -\frac{\partial\mathcal{H}}{\partial I_r}.
\end{aligned}$$

By satisfying the transversality conditions, $\sigma_i(t_f) = 0$, for each i within the range of 1 through 6, an analysis of the controls' behavior can be elucidated through the process of differentiating the Hamiltonian, $\mathcal{H}$, with respect to the optimal control triplet $(\mathbb{C}_1^*, \mathbb{C}_2^*, \mathbb{C}_3^*)$.

$$\frac{\partial\mathcal{H}}{\partial\mathbb{C}_i} = 0, \quad i = 1, 2, 3.$$

Then, the controls can be defined by implementing limitations on their values through suitable justifications.

$$\mathbb{C}_i^* = \begin{cases} 0, & \text{if } \Delta_i^* \le 0 \\ \Delta_i^*, & \text{if } 0 \le \Delta_i^* \le 1 \\ 1, & \text{if } \Delta_i^* \ge 1 \end{cases}$$

where

$$\begin{aligned}
\Delta_1^* &= \frac{(\alpha_m(\sigma_2-\sigma_1)+\alpha_s(\sigma_3-\sigma_1))SI_r}{B_1}, \\
\Delta_2^* &= \frac{(\sigma_2-\sigma_4)\theta_1 I_m + (\sigma_3-\sigma_4)\theta_1 I_s}{B_2}, \\
\Delta_3^* &= \frac{\Lambda\sigma_5 + \theta_3\sigma_6 I_r + \theta_3\sigma_5 S_r}{B_3}.
\end{aligned}$$

This completes the proof. □

The problem's numerical solution has been executed, and the efficacy of the implemented controls has been observed. The premise of this study is based on a 4-week optimal campaign, leveraging the values from Tables 1 and 2. The initial conditions are established as follows: $S(0) = 218{,}541{,}212$; $I_m(0) = 39$; $I_s(0) = 10$, $R(0) = 50$; $S_r(0) = 500{,}000$; and $I_r(0) = 10{,}000$. Positive weights are designated as follows: $A_1 = 3$; $A_2 = 6$; $A_3 = 9$; and $A_4 = 12$ and $B_1 = 2$; $B_2 = 4$; and $B_3 = 6$. By adopting a comprehensive array of controls, the ultimate objective is to minimize the count of victims while increasing the number of individuals who have successfully recovered. These outcomes are effectively demonstrated through graphical visualizations. Figure 9 presents the results of optimal control for estimated parameter values.

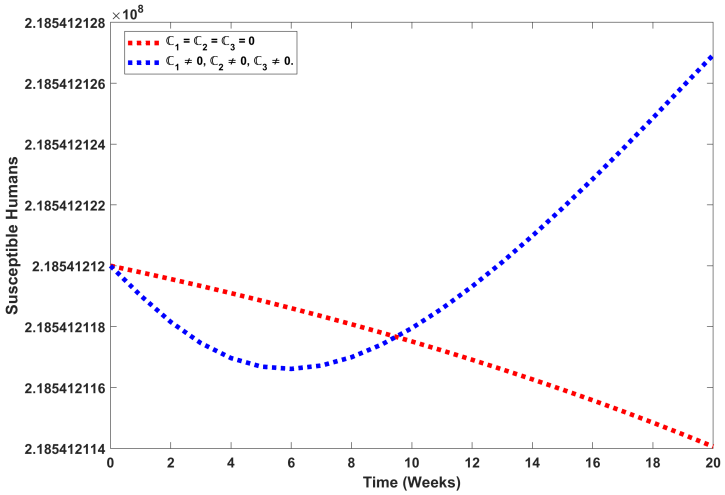

(**a**)

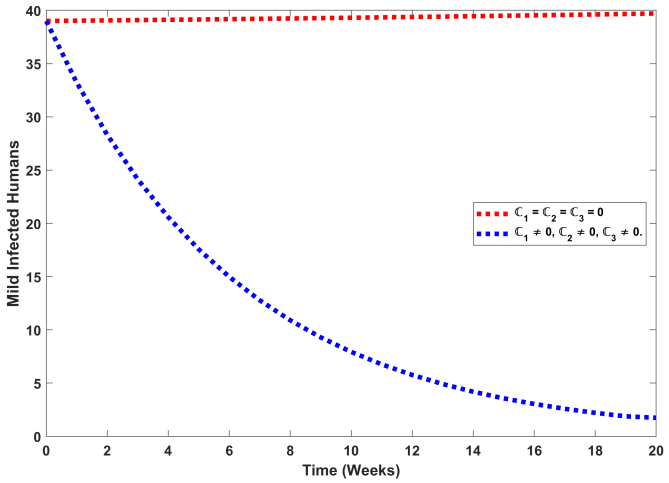

(**b**)

Figure 9. *Cont.*

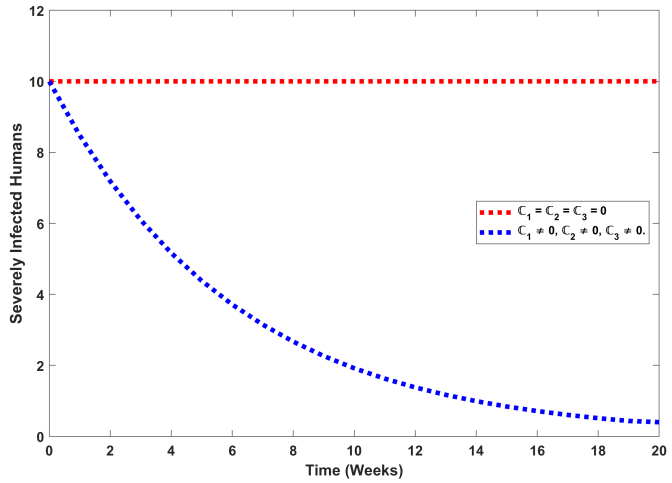

(**c**)

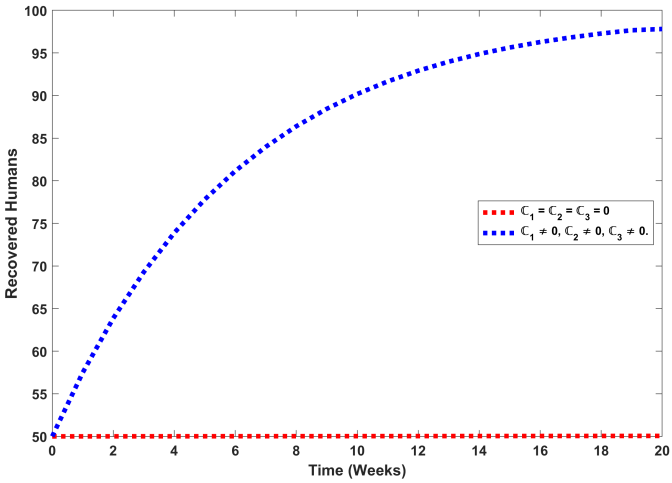

(**d**)

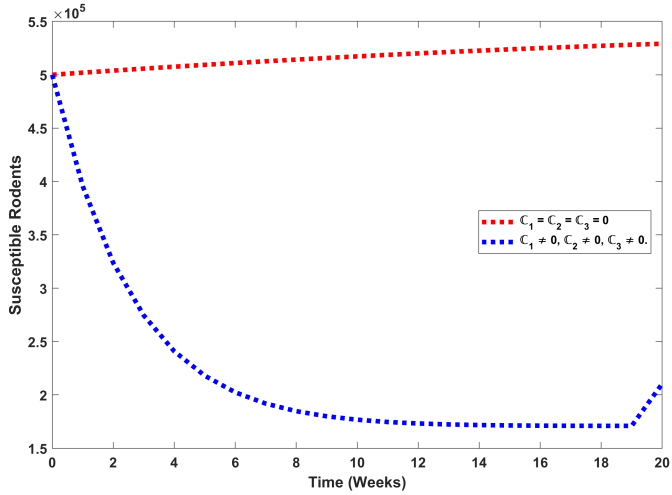

(**e**)

Figure 9. *Cont.*

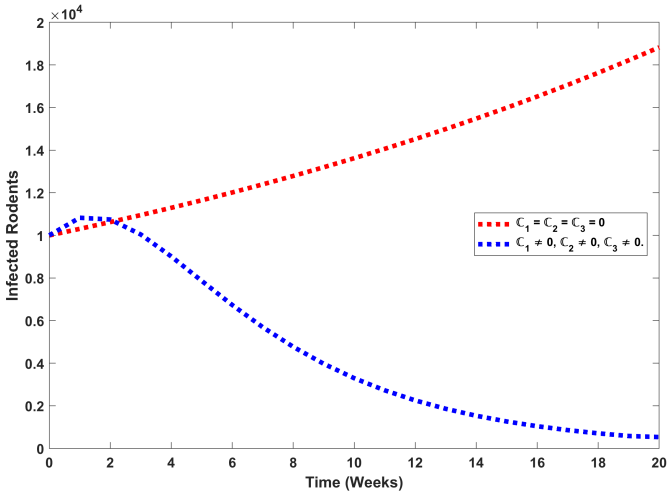

(**f**)

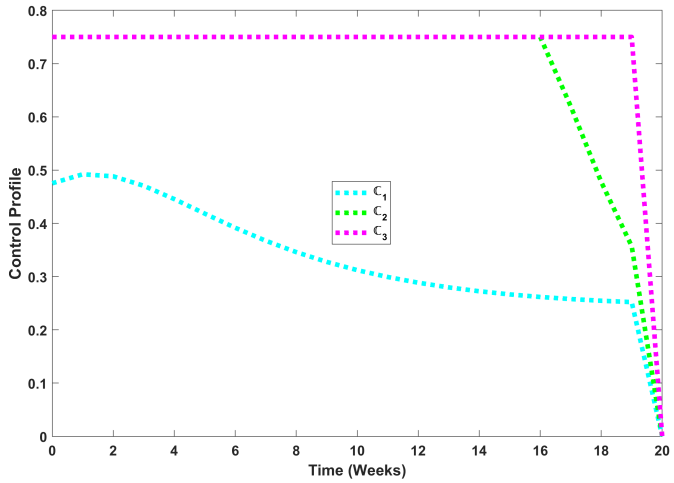

(**g**)

Figure 9. Implementation of controls $\mathbb{C}_1$, $\mathbb{C}_2$, and $\mathbb{C}_3$.

In Figure 9a, it can be seen that adopting preventive measures leads to a notable reduction in the susceptible human population, but after the 6th week, it starts to increase. This signifies that the shift of susceptible individuals into the infected group and subsequently into the recovered category has stopped.

Implementing control strategies gradually curtails the count of mildly and severely infected humans. This trend is evident in Figure 9b,c. The increased number of individuals recovering from the infection is clearly displayed in Figure 9d.

Moreover, after the integration of control efforts, Figure 9e demonstrates a decline in the susceptible rodent population. This suggests that rodents are moving into the infected category or are being removed from the community. Furthermore, Figure 9f highlights a significant reduction in infected rodents.

Numerical results illustrating the effectiveness of various optimal control measures in mitigating Lassa virus transmission are depicted in Figure 9g. These observations showcase the efficiency of each strategy in curtailing the spread of the virus within the community during specific time intervals. Precisely, Control $\mathbb{C}_1$ demonstrates a 48% efficacy initially, which remains effective until the 19th week. Control $\mathbb{C}_2$ exhibits a pattern of efficacy initially from 75%, followed by stabilization until the 16th week, and then decreases in effectiveness. Similarly, control $\mathbb{C}_3$ depicts a 75% efficacy that remains more stable and effective.

3. Conclusions

This article develops a mathematical model to provide valuable insights into the interaction between the virus' systemic behavior and its ability to trigger disabilities. The investigation of the infection-free equilibrium point's stability, coupled with the model's validation using real-world data, enhances the reliability and applicability of the findings.

Estimating the parameters and calculating the basic reproductive number add a quantitative dimension, helping to gauge the potential of the virus to spread within a population alongside the examination of weekly trends among subpopulations. Sensitivity analysis identifies key influencers driving transmission dynamics, emphasizing the substantial effects of threshold parameters through the visual representation of informative contour plots.

The rigorous case analysis and comprehensive literature review exhibit a direct correlation between Lassa fever and impairments like hearing loss, encephalitis, neuropsychiatric symptoms, ataxia, seizures, meningitis, and coma. Recognizing these neurological consequences underscores the urgent need for effective control measures to mitigate the impact of the disease on patients' long-term health.

This study creatively suggests the use of nanotechnology as a targeted intervention, diagnostic tool, and protective measure against neurological damage caused by the Lassa virus. The amalgamation of epidemiological proficiency with nanotechnology presents an innovative approach to alleviating neurological consequences and bolstering outbreak responses. Through the fusion of mathematical modeling, epidemiological investigation, and nanotechnology applications, this all-encompassing research embraces a multidimensional methodology for addressing the complexities linked to the Lassa virus, offering valuable insights for policymakers, researchers, and public health authorities.

Author Contributions: Conceptualization, Y.R. and K.G.; methodology, H.A.; software, K.G.; validation, B.M.F.; formal analysis, Y.R. and B.M.F.; investigation, H.A. and K.G.; resources, B.M.F.; data curation, M.A.; writing—original draft preparation, Y.R.; writing—review and editing, A.U.A.; visualization, M.A.; supervision, A.U.A.; project administration, B.M.F.; funding acquisition, A.U.A. All authors have read and agreed to the published version of the manuscript.

Funding: This work was funded by the King Salman Center for Disability Research through Research Group no KSRG-2024-184.

Data Availability Statement: The data used to support the findings of this study are included within the article.

Acknowledgments: The authors extend their appreciation to the King Salman Center for Disability Research for funding this work through Research Group no KSRG-2024-184.

Conflicts of Interest: The authors declare no conflicts of interest.

References

1. Ojo, M.M.; Gbadamosi, B.; Benson, T.O.; Adebimpe, O.; Georgina, A. Modeling the Dynamics of Lassa Fever in Nigeria. *J. Egypt. Math. Soc.* **2021**, *29*, 16. [CrossRef]
2. Onah, I.S.; Collins, O.C. Dynamical System Analysis of a Lassa Fever Model with varying Socioeconomic Classes. *J. Appl. Math.* **2020**, *2020*, 2601706. [CrossRef]
3. Uwishema, O.; Alshareif, B.A.; Yousif, M.Y.; Omer, M.E.; Sablay, A.L.; Tariq, R.; Zahabioun, A.; Mwazighe, R.M.; Onyeaka, H. Lassa Fever Amidst the COVID-19 Pandemic in Africa: A Rising Concern, Efforts, Challenges, and Future Recommendations. *J. Med. Virol.* **2021**, *93*, 6433–6436. [CrossRef] [PubMed]
4. World Health Organization. Lassa Fever in Nigeria. 2022. Available online: https://www.who.int/emergencies/disease-outbreak-news/item/lassa-fever---nigeria (accessed on 22 October 2024).
5. Khan, S.H.; Goba, A.; Chu, M.; Roth, C.; Healing, T.; Marx, A.; Fair, J.; Guttieri, M.C.; Ferro, P.; Imes, T.; et al. New Opportunities for Field Research on the Pathogenesis and Treatment of Lassa Fever. *Antivir. Res.* **2008**, *78*, 103–115. [CrossRef]
6. Okokhere, P.O.; Ibekwe, T.S.; Akpede, G.O. Sensorineural Hearing Loss in Lassa Fever: Two Case Reports. *J. Med. Case Rep.* **2009**, *3*, 1–3. Available online: http://www.jmedicalcasereports.com/content/3/1/36 (accessed on 22 October 2024). [CrossRef]

7. Cummins, D.; McCormick, J.B.; Bennett, D.; Samba, J.A.; Farrar, B.; Machin, S.J.; Fisher-Hoch, S.P. Acute Sensorineural Deafness in Lassa fever. *JAMA* **1990**, *264*, 2093–2096. Available online: https://jamanetwork.com/journals/jama/article-abstract/383705 (accessed on 22 October 2024). [CrossRef] [PubMed]
8. Solbrig, M.V. *The Arenaviridae: Lassa Virus and Central Nervous System Diseases*; Springer: Berlin/Heidelberg, Germany, 1993.
9. Macher, A.M.; Wolfe, M.S. Historical Lassa Fever Reports and 30-year Clinical Update. *Emerg. Infect. Dis.* **2006**, *12*, 835. [CrossRef]
10. Okokhere, P.; Bankole, I.; Akpede, G. Central Nervous System Manifestations of Lassa Fever in Nigeria and the Effect on Mortality. *J. Neurol. Sci.* **2013**, *333*, e604. [CrossRef]
11. Ramzan, Y.; Awan, A.U.; Ozair, M.; Hussain, T.; Mahat, R. Innovative Strategies for Lassa Fever Epidemic Control: A Groundbreaking Study. *AIMS Math.* **2023**, *8*, 30790–30812. [CrossRef]
12. Din, A. Bifurcation Analysis of a Delayed Stochastic HBV Epidemic Model: Cell-to-cell Transmission. *Chaos Solitons Fractals* **2024**, *181*, 114714. [CrossRef]
13. Guedri, K.; Ramzan, Y.; Awan, A.U.; Fadhl, B.M.; Ali, B.; Oreijah, M. Rabies-Related Brain Disorders: Transmission Dynamics and Epidemic Management via Educational Campaigns and Application of Nanotechnology. *Eur. Phys. J. Plus* **2024**, *139*, 49. [CrossRef]
14. Khan, F.M.; Khan, Z.U.; Abdullah. Numerical Analysis of Fractional Order Drinking Mathematical Model. *J. Math. Tech. Model.* **2024**, *1*, 11–24. [CrossRef]
15. Guedri, K.; Ramzan, Y.; Awan, A.U.; Fadhl, B.M.; Oreijah, M. Modeling Transmission Patterns and Optimal Control through Nanotechnology: A Case Study of Malaria Causing Brain Disabilities. *J. Disabil. Res.* **2024**, *3*, 20230061. [CrossRef]
16. Khan, W.A.; Zarin, R.; Zeb, A.; Khan, Y.; Khan, A. Navigating Food Allergy Dynamics via a Novel Fractional Mathematical Model for Antacid-Induced Allergies. *J. Math. Tech. Model.* **2024**, *1*, 25–51. [CrossRef]
17. Hamam, H.; Ramzan, Y.; Niazai, S.; Gepreel, K.A.; Awan, A.U.; Ozair, M.; Hussain, T. Deciphering the Enigma of Lassa Virus Transmission Dynamics and Strategies for Effective Epidemic Control through Awareness Campaigns and Rodenticides. *Sci. Rep.* **2024**, *14*, 18079. [CrossRef]
18. Ain, Q.T. Nonlinear Stochastic Cholera Epidemic Model under the Influence of Noise. *J. Math. Tech. Model.* **2024**, *1*, 52–74. [CrossRef]
19. Shah, S.M.A.; Tahir, H.; Khan, A.; Khan, W.A.; Arshad, A. Stochastic Model on the Transmission of Worms in Rireless Sensor Network. *J. Math. Tech. Model.* **2024**, *1*, 75–88. [CrossRef]
20. Ndenda, J.; Njagarah, J.; Shaw, S. Influence of Environmental Viral Load, Interpersonal Contact and Infected Rodents on Lassa Fever Transmission Dynamics: Perspectives from Fractional-Order Dynamic Modelling. *AIMS Math.* **2022**, *7*, 8975–9002. [CrossRef]
21. Barua, S.; Denes, A.; Ibrahim, M.A. A Seasonal Model to Assess Intervention Strategies for Preventing Periodic Recurrence of Lassa Fever. *Heliyon* **2021**, *7*, e07760. [CrossRef]
22. Van den Driessche, P.; Watmough, J. Reproduction Numbers and Sub-Threshold Endemic Equilibria for Compartmental Models of Disease Transmission. *Math. Biosci.* **2002**, *180*, 29–48. [CrossRef]
23. Obiajulu, E.F.; Omame, A.; Inyama, S.C.; Diala, U.H.; AlQahtani, S.A.; Al-Rakhami, M.S.; Alawwad, A.M.; Alotaibi, A.A. Analysis of a non-integer order mathematical model for double strains of dengue and COVID-19 co-circulation using an efficient finite-difference method. *Sci. Rep.* **2023**, *13*, 17787. [CrossRef]
24. Usman, M.; Abbas, M.; Omame, A. Analysis of the solution of a model of sars-cov-2 variants and its approximation using two-step lagrange polynomial and euler techniques. *Axioms* **2023**, *12*, 480. [CrossRef]
25. Kumar, P.; Govindaraj, V.; Erturk, V.S.; Nisar, K.S.; Inc, M. Fractional Mathematical Modeling of the Stuxnet Virus along with an Optimal Control Problem. *AIN Shams Eng. J.* **2023**, *14*, 102004. [CrossRef]
26. Collins, O.; Govinder, K. Stability Analysis and Optimal Vaccination of a Waterborne Disease Model with Multiple Water Sources. *Nat. Resour. Model.* **2016**, *29*, 426–447. [CrossRef]
27. Castillo-Chavez, C.; Blower, S.; van den Driessche, P.; Kirschner, D.; Yakubu, A.A. *Mathematical Approaches for Emerging and Re-emerging Infectious Diseases: Models, Methods, and Theory*; Springer Science & Business Media: New York, NY, USA, 2002.
28. Macrotrends. Nigeria Life Expectancy. 2022. Available online: https://www.macrotrends.net/countries/NGA/nigeria/life-expectancy (accessed on 22 October 2024).
29. World Bank. Total Population in Nigeria. 2022. Available online: https://data.worldbank.org/indicator/SP.POP.TOTL?locations=NG (accessed on 22 October 2024).
30. Chitnis, N.; Hyman, J.M.; Cushing, J.M. Determining Important Parameters in the Spread of Malaria through Sensitivity Analysis of a Mathematical Model. *Bull. Math. Biol.* **2008**, *70*, 1272–1296. [CrossRef]
31. Pontryagin, L.S.; Boltyanskii, V.G.; Gamkrelidze, R.V.; Mishchenko, E.F. *Mathematical Theory of Optimal Processes*; CRC Press: Boca Raton, FL, USA, 1987.
32. Fleming, W.H.; Rishel, R.W. *Deterministic and Stochastic Optimal Control*; Springer Science & Business Media: New York, NY, USA, 2012.
33. Adepoju, O.A.; Olaniyi, S. Stability and Optimal Control of a Disease Model with Vertical Transmission and Saturated Incidence. *Sci. Afr.* **2021**, *12*, e00800. [CrossRef]